Sensors and Materials, Vol. 21, No. 1 (2009) 1–12
MYU Tokyo

S & M 0744

Effects of Pressure on GaAs/In_xGa_{1-x}As/AlAs Resonant Tunneling Structures

Binzhen Zhang, Zhaomin Tong*, Chenyang Xue and Wendong Zhang

Room 401, National Key Laboratory for Electronic Measurement Technology,
Key Laboratory of Instrumentation Science & Dynamic Measurement,
Ministry of Education, North University of China, Taiyuan 030051, P.R. China

(Received December 11, 2007; accepted September 19, 2008)

Key Words: stress, GaAs/In_xGa_{1-x}As/AlAs, RTS, Raman spectroscopy, meso-piezoresistive effect

The characteristics of GaAs/In_xGa_{1-x}As/AlAs double-barrier resonant tunneling structures (DBRTSs) subjected to pressure are discussed in this paper. DBRTS is grown by molecular beam epitaxy (MBE) on a [001]-oriented semi-insulating substrate, and the resonant tunneling structure (RTS) is processed successfully using an air-bridge structure and AuGe/Ni/Au metallization with a clear negative differential resistance (NDR) phenomenon. Because of the meso-piezoresistive effect of DBRTS, uniaxial, compressive stresses, which are determined by Raman spectroscopy, induce obvious I-V curve shifts: to more positive voltages (under stress along the [110] orientation) and to more negative voltages (under stress along the $[1\bar{1}0]$ orientation). The meso-piezoresistive sensitivities are approximately -1.51×10^{-9} Pa^{-1} (under [110] stress) and 3.03 $\times10^{-9}$ Pa^{-1} (under $[1\bar{1}0]$ stress), which are about one order higher than those of silicon. For the oscillator with RTS, the variety of its relaxation oscillation frequency (approximately –17.9 kHz/MPa) under stress is also presented and the mechanism is discussed.

1. Introduction

In recent years, with rapid developments in molecular beam epitaxy (MBE) and metallorganic chemical vapor deposition (MOCVD) and the technologies of etching methods, many types of quantum well material can be grown and fabricated.[1–3] A resonant tunneling diode (RTD) is an example of such quantum well material with a negative differential resistance (NDR) effect on the current-voltage (I-V) characteristics, and it has been widely used in electronic and photonic devices over the last decade. Oscillations of up to 712 GHz have been reported and several applications of RTD for multivalued logic have been proposed;[4–6] the latter focused on the utilization of the unique electronic and optic properties of these devices for lasers, detectors and modulators in the infrared-to-visible wavelength range,[7,8] and high-speed optically switched electronic devices.[9,10]

*Corresponding author: e-mail: tong-zhaomin@tom.com

Pressure or stress plays a very important role in the investigation of the transport properties of semiconductor materials and offers a possibility of designing heterostructure devices with customized performances.[11,12] All III-V compounds are piezoelectric owing to the polar character of the bonds between their different atoms. The piezoelectric effect can cause internal electric fields in III-V semiconductor heterostructures if the polarization fields have a nonvanishing component in the direction perpendicular to the interfaces and differ in magnitude and/or sign between the different layers. For GaAs/$In_xGa_{1-x}As$/AlAs double-barrier resonant tunneling structures (DBRTSs), the I-V curves will change under external stress; the well-known effects are as follows: energy band gap variation with hydrostatic pressure, stress-induced piezoelectric field in III-V compound semiconductors, change in the band edge curvature, and band edge splitting with uniaxial pressure.[13] These effects have been used for designing novel sensors.[14,15]

The piezoresistive coefficients of doped-silicon are at on the 10^{-11} Pa^{-1} order,[16] which induces the low sensitivity of traditional sensors based on the above effects. Thus, under some high-sensitivity condition, new materials with high piezoresistive coefficients are needed. In this paper, we discuss the measurements of the static uniaxial stress applied on a GaAs/$In_xGa_{1-x}As$/AlAs resonant tunneling structure (RTS) along the [110] and $[1\bar{1}0]$ directions. GaAs/$In_xGa_{1-x}As$/AlAs thin films are grown by MBE on a [001]-oriented GaAs semi-insulating substrate, and the RTS is fabricated with an air-bridge structure. Under external stress, the RTS's I-V curves show a positive ([110] orientation) and/or negative ($[1\bar{1}0]$ orientation) shift; its relaxation oscillation frequency also shows a change, and the reasons for all these observations are discussed. The 10^{-9} Pa^{-1} meso-piezoresistive sensitivity indicates that these structures can be used for designing high-sensitivity sensors, and its frequency output characteristics (approximately –17.9 kHz/MPa) imply its potential applications under half-digital conditions.

2. Design and Fabrication

The current of RTS consists of two competitive parts, defined as[17]

$$J = J_{RT} + J_{EX}, \tag{1}$$

where J_{RT} is the resonant tunneling current, which induces the NDR effect of RTS directly, and J_{EX} is the excess current; it is also composed of two parts: inelastic tunneling current and the thermocurrent J_{TH}. J_{TH} is affected markedly by the change in temperature; the NDR effect can even be covered up by J_{TH} at high temperature. The purpose of the designer is to obtain maximum J_{RT} and minimum J_{EX}.

A GaAs/$In_xGa_{1-x}As$/AlAs resonant tunneling material is grown in a gas source MBE Riber 32P system on semi-insulating GaAs substrates oriented along [001] ±0.1°. The substrates are heated to 350°C for approximately 1 h before being transferred into the growth chamber. The detailed structures and dimensions are shown in Table 1. On the semi-insulated GaAs substrate is the 1-µm-thick heavily doped n-type (3×10^{18} cm^{-3}) GaAs collector ohmic contact layer, followed by 10-nm-thick heavily doped n-type (10^{17} cm^{-3}) GaAs collector layer; 5-nm-thick GaAs undoped layers are grown to

Table 1
Structures and dimensions of $GaAs/In_xGa_{1-x}As/AlAs$ DBRTS.

Depth (nm)	Material	Layer
500	N^+-GaAs(3×10^{18} cm^{-3})	ohmic contact
10	N^+-GaAs(10^{17} cm^{-3})	emitter
5	GaAs	
5	$In_{0.1}Ga_{0.9}As$	well before barrier
0.5	GaAs	
1.7	AlAs	barrier
0.5	GaAs	
4	$In_{0.1}Ga_{0.9}As$	well
0.5	GaAs	
1.7	AlAs	barrier
0.5	GaAs	
5	$In_{0.1}Ga_{0.9}As$	well before barrier
5	GaAs	
10	N^+-GaAs(10^{17} cm^{-3})	collector
1000	N^+-GaAs(3×10^{18} cm^{-3})	ohmic contact
	3" N^+/SI-GaAs substrate	

prevent the diffusion of doped layers and to increase barrier height. 5-nm-thick InGaAs subwells are grown, which induces a decrease in J_{RT}, and also restrains the thermo current J_{TH}. The restrain of J_{TH} is much greater than the decrease in J_{RT}, and the RTS has a much lower peak current, but the peak-valley ratio (PVR) of the current can be improved considerably. The double-barrier single-well $GaAs/In_xGa_{1-x}As/AlAs$ sandwich structures are chucked at the center with a 1.7-nm-thick AlAs high-band energy barrier layer to decrease J_{TH} and a 5-nm-deep GaAs/InGaAs/GaAs well; finally, a 10-nm-thick heavily doped *n*-type (10^{17} cm^{-3}) GaAs emitter layer is grown, with a 500-nm-thick heavily doped *n*-type (3×10^{18} cm^{-3}) GaAs emitter ohmic contact layer above it. Figure 1 shows the transmission electron microscopy (TEM) image of the $GaAs/In_xGa_{1-x}As/AlAs$ heterostructures.

We begin the fabrication of RTS with 8×8 μm^2 square emitter mesa etching using inductively coupled plasma (ICP), followed by AuGe/Ni ohmic contact deposition, patterning, and annealing at 450°C for 30 min (15% H_2 and 85% N_2). After collector mesa photolithography and the deposition of Si_3N_4 as insulating layer, the electrodes are formed with an air-bridge structure to provide measurements under applied bias. Figure 2 shows a scanning electron microscopy (SEM) image of the fabricated RTS.

3. Experimental Methods

Stress change can be calculated by Raman spectroscopy accurately and with no damage.[18] When the sample is subjected to pressure, the energy of vibration changes and the Raman band shifts to either higher (compression) or lower (expansion) energy.

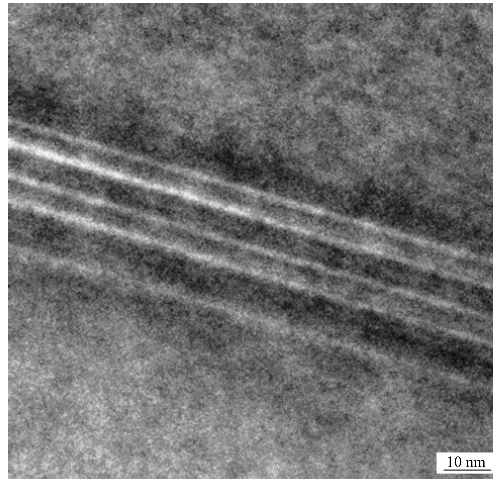

Fig. 1. TEM image of GaAs/$In_xGa_{1-x}As$/AlAs heterostructures.

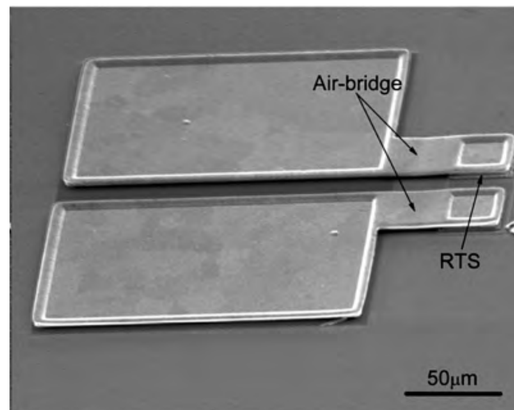

Fig. 2. SEM image of RTS.

From the shift of the Raman band, stress change can be determined. For backscattering from the [001] plane, the relationship between the Raman band shift and the stress is represented as

$$\Delta\varpi = \frac{\lambda_3}{2\varpi_0} = \frac{q\,(S_{11} + S_{12}) + pS_{12}}{2\varpi_0}\,\sigma_{XX}, \tag{2}$$

where p and q are the phonon deformation potentials (PDPs), S_{11} and S_{12} are elements of the compliance tensor of the crystal, and σ_{XX} is the stress.

For the [001]-oriented GaAs, the Raman band shift and the stress have the following relation;

$$\sigma_{XX} = -\ 576\Delta\varpi. \qquad (3)$$

Here, "–" denotes that the stress is a tensile stress.

We have used an inVia Raman spectrometer (RENISHAW inc.) to measure the stress change. The GaAs/$In_xGa_{1-x}As$/AlAs DBRTS is positioned on an object stage, and the stress is applied using a movement knob device. By using two conducting wires, the electrodes of RTS are connected with an Agilent 4156C semiconductor characteristic analyzer and an oscillator circuit. The I-V curves are calculated using Agilent 4156C, and the change in relaxation oscillation frequency is measured using the oscillator circuit. Figure 3 shows the schematic diagram of the measurement system.

4. Results and Discussion

Figures 4 and 5 are the I-V curves of RTS with pressure variation measured using the inVia Raman spectrometer (RENISHAW inc.) and Agilent 4156C semiconductor analyzer; pressure is brought along the [110] and [$1\bar{1}0$] orientations by a movement knob device. From the examination of the RTS's I-V curves, the clearest effect is their shifts. When transverse stress along the [110] orientation is applied to the RTS, we find that the I-V curves shift to more positive values, as shown in Fig. 4. For stress along the [$1\bar{1}0$] orientation, the I-V curves are found to shift to more negative values, as shown in Fig. 5.

Plots of the normalized relative resistance versus external stresses along the [110] and [$1\bar{1}0$] orientations are shown in Fig. 6. Here, we have a 10-MPa-stress error bar that

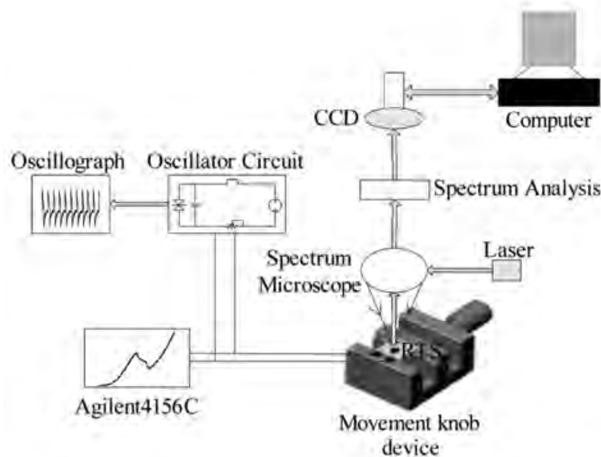

Fig. 3. Schematic diagram of pressure measurement system.

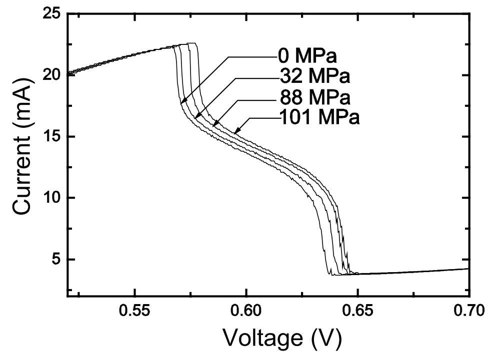

Fig. 4. I-V curve change with pressure applied along [110] orientation.

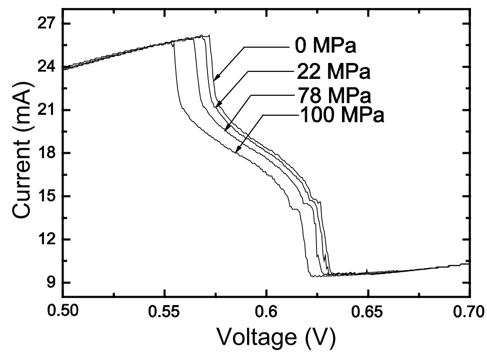

Fig. 5. I-V curve change with pressure applied along $[1\bar{1}0]$ orientation.

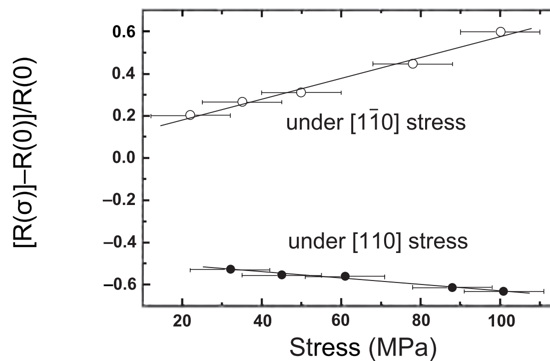

Fig. 6. Relative resistance changes under [110] and $[1\bar{1}0]$ stresses.

is induced by the stochastic error of the Raman spectrometer.(18) The linear sensitivity (S) of relative resistance with stress change can be defined as

$$S = \frac{\Delta R}{R(0)\cdot\sigma} = \frac{R(\sigma) - R(0)}{R(0)\cdot\sigma} = \frac{\dfrac{U(ref)}{I(\sigma)} - \dfrac{U(ref)}{I(0)}}{\dfrac{U(ref)}{I(0)}\cdot\sigma} = \left.\frac{I(0) - I(\sigma)}{I(\sigma)\cdot\sigma}\right|_{U(ref)}, \quad (4)$$

where $I(\sigma)$ and $I(0)$ are the RTS's currents in the presence and absence of external stress, respectively; σ is the external stress. For different reference voltages, S will change, and in the NDR region, the largest S can be obtained.(19)

From eq. (4), the largest values of S (at $U_{ref} = 0.64$ V) are approximately -1.51×10^{-9} Pa^{-1} (under [110] stress) and 3.03×10^{-9} Pa^{-1} (under [1$\bar{1}$0] stress), which are about one order higher than those of silicon; the difference is mainly attributed to the asymmetry of material growth.

Another characteristic of RTS under pressure is its relaxation oscillation frequency change when biased in NDR. Bias voltage is supplied using MAX8526, which is a low-dropout linear regulator, and its output voltage accuracy is ±1.4% between 0 and 85°C. The pressure is applied along the [110] orientation, and the variation in oscillation frequency with pressure is shown in Fig. 7.

The change in oscillation frequency can be calculated using

$$S_f = \frac{\Delta f}{\sigma} = \frac{f_\sigma - f_0}{\sigma}. \quad (5)$$

where f_σ is the frequency under stress, f_0 is the intrinsic frequency, and σ is the stress. According to eq. (5), the linear variation is approximately –17.9 KHz/MPa; here, "–" denotes that the frequency decreases with applied pressure.

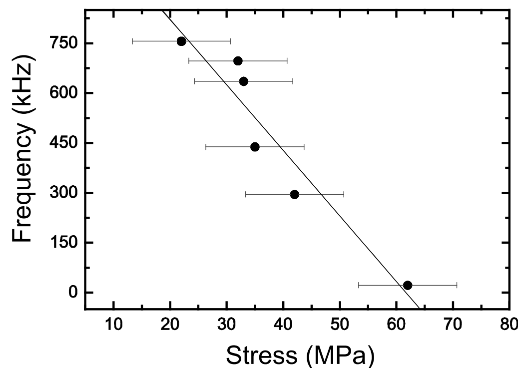

Fig. 7. Variety of oscillation frequencies with applied pressure.

4.1 *Meso-piezoresistive effect of RTS*

The observed I-V curves' change and the calculated ~10^{-9} Pa^{-1} meso-piezoresistive sensitivity of RTS can be illustrated qualitatively. According to Wen *et al.*,[20] the external strain in superlattices results from the mechanical interaction between two adjacent layers. At room temperature and normal pressure, if the interference is zero, the tetragonal distortion can be written as

$$\Delta\varepsilon' = \Delta\tilde{\varepsilon}[\beta - \beta^{\parallel}]\Delta T_g, \tag{6}$$

where ΔT_g is the difference between growth temperature and room temperature, β is the thermal expansion coefficient at room temperature, $\beta^{\parallel}$ is the in-plane linear thermal expansion coefficient, and $\Delta\tilde{\varepsilon}$ is determined by the elastic constant and growth direction of superlattices. In general cases, the external strain can be written as

$$\Delta\varepsilon = \Delta\varepsilon' + \delta\varepsilon, \tag{7}$$

where $\delta\varepsilon$ depends on growth interference and can be calculated and measured quantitatively.

Because of the piezoelectric constant difference between the AlAs and GaAs layers, when subjected to stress fields, polarization charges are induced at the interfaces in each layer and generate piezoelectric fields in the barriers and the well of the RTS. A general description of the built-in electric field and strain can be expressed as

$$E = \mathrm{A}\Delta\varepsilon, \tag{8}$$

where A is a constant. The built-in electric field will result in the formation of the valence band offset difference ΔV_{B} on the two sides of a barrier, which can be defined as

$$\Delta V_{\mathrm{B}} = e \begin{cases} \sum_{i=1}^{2} \int_0^{hi} E_i(x)\,dx \quad \text{and} \quad 0, & e'_1 e'_2 > 0 \\ \int_0^{h1} E_1(x)\,dx \quad \text{and} \quad \int_0^{h2} E_2(x)\,dx, & e'_1 e'_2 < 0 \\ \int_0^{h} E(x)\,dx \quad \text{and} \quad 0, & e'_1 e'_2 = 0 \end{cases}, \tag{9}$$

where e is the electron charge, e'_1 and e'_2 are the piezoelectric coefficients for the two adjacent layers, and h_i is the thickness of the piezoelectric layer (i = 1, 2).

When under [110] stress, because the piezoelectric constant of the AlAs layer is larger than that of the GaAs layer,[21] the direction of the electric field is antiparallel to that of the applied electric field E_a for positive bias; therefore, a higher applied voltage is required to realize the resonant tunneling condition, as shown in Fig. 8(a). However, under [1$\bar{1}$0] stress, polarization charges have the opposite sign at each heterointerface compared with the [110] case. Hence, more negative applied voltages are required to realize the resonant tunneling condition, as shown in Fig. 8(b).[22]

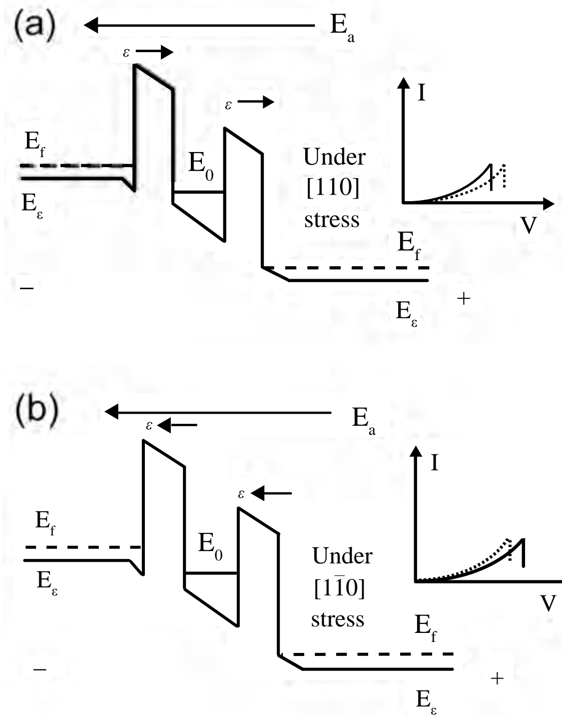

Fig. 8. Schematic band diagram and I-V curves for [001]-oriented RTS under stress: (a) along [110] direction, and (b) along [1$\bar{1}$0] direction. The solid I-V curve represents current without applied stress and the dotted curve represents current with applied stress.[22]

To simplify the theoretical expression, the Landauer resistance is defined as

$$R_L = \frac{h}{e^2}\frac{R(\Delta V_B)}{T(\Delta V_B)}. \tag{10}$$

From eqs. (6) to (10), we know that R_L can be written as a function of the strain $\Delta\varepsilon$:

$$R_L = f(\Delta\varepsilon). \tag{11}$$

This is a mathematical expression for the meso-piezoresistive effect, and therefore, it can be calculated qualitatively.

4.2 *Oscillation frequency change under stress*

For an oscillator with RTS, it consists of a voltage supply, a serial inductor, and a capacitor in parallel,[15] as shown in Fig. 9. When RTS is biased in its NDR region, the principle of its relaxation oscillation can be explained as follows, as shown in Fig. 10.

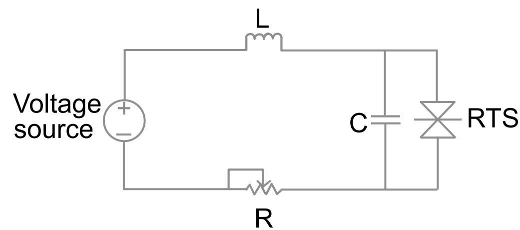

Fig. 9. Equation circuit of oscillator with RTS.

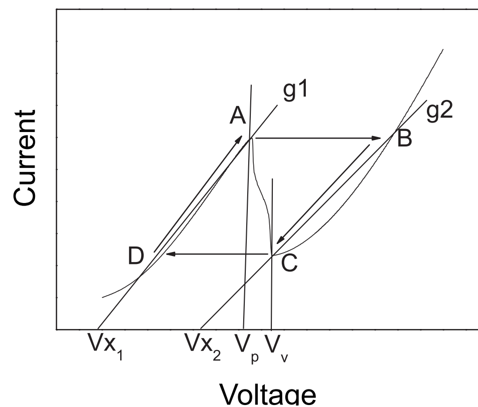

Fig. 10. Working mechanism of relaxation oscillation.

(1) First, current rises untill it reaches its peak value (Point A).
(2) The serial inductance, parallel capacitor and NDR force the diode to switch from A to B. The inductance maintains the current while the capacitor takes up the current difference and therefore increases the RTS's voltage. A fast switching from A to B occurs.
(3) The voltage reached is above the bias point and cannot be maintained by the voltage source. Therefore, the voltage decreases with a time constant determined through the inductor and the nonlinear RTS's positive resistance.
(4) If the valley voltage (C) is reached, a fast switch to D takes place.
The diode current increases while the inductor current remains constant. The current difference is supplied by the capacitor.

By the four steps above, when the bias voltage is in RTS's NDR, relaxation oscillation occurs.

For the oscillation circuit in Fig. 9, because the corresponding switching time from A to B and C to D is very short compared with those from B to C and D to A, the capacitor can be neglected. Therefore, we only have to calculate the time needed for the D to A and B to C transitions. The following equation can be obtained;

$$V_0 = Ri_d + L\ \frac{di_d}{dt} + V_d\ . \tag{12}$$

where V_d and i_d are the bias voltage and current flow in the RTS, respectively.

The next simplification will be to approximate the I-V curve between D to A and B to C through linear functions, so that g is constant in the two positive resistance regions. The equation can then be easily solved using the following assumption:

$$i_d = gV_d - gV_x. \tag{13}$$

Thus, eq. (12) can be written as

$$V_0 = (Rg + 1)\,V_d - RgV_x + gL\ \frac{dV_d}{dt}. \tag{14}$$

For solving the differential equation, a boundary condition is necessary. If the transition from D to A (B to C) is set to begin at $t = 0$ and the corresponding voltage at D (B) is V_D (V_B), the solution for the entire oscillation period, assuming that gR is much less than 1, is

$$t = g_1L\left[\ln\left(\frac{V_D - Rg_1V_{x1} - V_0}{V_P - Rg_1V_{x1} - V_0}\right)\right] + g_2L\left[\ln\left(\frac{V_B - Rg_2V_{x2} - V_0}{V_v - RgV_{x2} - V_0}\right)\right]. \tag{15}$$

Looking at eq. (15), oscillation frequency is determined using L, R, V_P, and V_v. Because of the meso-piezoresistive effect of RTS, which will alter its I-V curves as illustrated above, i.e., R, V_P, and V_v, oscillation frequency will change.

5. Conclusion

The effects of pressure on GaAs/In_xGa_{1-x}As/AlAs DBRTS have been investigated. TEM has proved that the structures of GaAs/In_xGa_{1-x}As/AlAs thin films grown by MBE are corrected, and measurement results show that these multilayer films have a clear NDR effect. Pressure has significant effects on the characteristics of RTS; the evident effects are the I-V curve shifts and the change in relaxation oscillation frequency. Measurement results show that resonant tunneling structures are very sensitive to external pressure; the oscillation frequency has a –17.9 kHz/MPa change with [110] external stress, and the -1.51×10^{-9} Pa^{-1} (under [110] stress) and 3.03×10^{-9} Pa^{-1} (under [$1\bar{1}0$] stress) meso-piezoresistive sensitivities are one order higher than those of silicon. These structures can be used for designing some novel high-sensitivity and high-frequency output sensors. Some significant problems needed to be solved for these structures are the requirement of a stable voltage supply and their temperature dependence.

Acknowledgement

This work was supported by the National Natural Science Foundation of China under grant Nos. 50775209 and 50535030, and the New Century Excellent Talents (NCET) program of the university.

References

1 M. Kaniewska and O. Engström: Mater. Sci. Eng. C **27** (2007) 1069.
2 S. M. Kim, Y. Furukawa and H. Yonezu: Cryst. Growth **293** (2006) 359.
3 C. J. Anthony, C. A. Helen and R. C. Paul: Surf. Coat. Technol. **201** (2007) 9046.
4 E. R. Brown, J. R. Soderstorm, C. D. Parker, L. J. Mahoney, K. M. Molvar and T. C. McGill: Appl. Phys. Lett. **58** (1991) 2291.
5 J. Soderstrom and T. G. Anderson: IEEE Electron Device Lett. **9** (1988) 2163.
6 Z. X. Yan and M. J. Deen: IEEE J. Solid-St. Circ. **27** (1992) 1198.
7 B. F. Levine: J. Appl. Phys. **74** (1993) R1.
8 A. Rogalski: Infrared Phys. Technol. **38** (1997) 295.
9 H. S. Li.: Appl. Phys. Lett. **65** (1994) 2999.
10 T. S. Moise, Y. Kao, L. D. Garrett and J. C. Campbell: Appl. Phys. Lett. **66** (1995) 1104.
11 H. Morkoc, B. Sverdlov and G. B. Gao: Proc. IEEE **81** (1993) 493.
12 P. S. Peercy: AT&T Tech. J. November/December (1991) 49.
13 S. C. Jain, M. Wilander and H. Maes: Semicond Sci. Technol. **11** (1996) 641.
14 K. Fobelets, R. Vounckx and G. Borghs: J. Micromech. Microeng. **4** (1994) 123.
15 K. Mutamba: IEEE Trans. Instrum. Meas. **48** (1999) 1333.
16 B. Stark: MEMS Reliability Assurance Guidelines for Space Applications (JPL Publishing, California, 1999) Chap. 4.
17 J. N. Schulman and H. J. Los Santos: IEEE Electron Device Lett. **17** (1996) 220.
18 S. Sang, C. Xue and W. Zhang: Solid State Phenom. **121–123** (2007) 943.
19 W. Zhang, C. Xue, J. Xiong, B. Xie, T. Wei and Y. Chen: Indian J. Pure Appl. Phys. **45** (2007) 294.
20 T. D. Wen, L. P. Xu and J. J. Xiong: Solid State Phenom. **121–123** (2007) 619.
21 S. Adachi: J. Appl. Phys. **58** (1985) R1.
22 K. Fricke: J. Micromech. Microeng. **3** (1993) 131.